TASK QUARTERLY 9 No 4, 461–473

NUMERICAL MODELLING OF ELASTO-VISCOPLASTIC BODNER-PARTOM CONSTITUTIVE EQUATIONS

ANDRZEJ AMBROZIAK

Department of Structural Mechanics,
Faculty of Civil and Environmental Engineering,
Gdansk University of Technology,
Narutowicza 11/12, 80-952 Gdansk, Poland
ambrozan@pg.gda.pl

(Received 14 July 2005)

Abstract: The aim of the paper is to propose an FE procedure for static and dynamic nonlinear analysis including elasto-viscoplastic constitutive equations of the Bodner-Partom model. Basic equations of the constitutive model are given with the flow graph used in the FE procedure. The proposed procedure has been applied in the MSC.Marc commercial system with a user-defined UVSCPL subroutine that enables application to a wide range of varied finite elements. A number of simple problems of static and dynamic analysis are presented to show the accuracy of this approach. The numerical simulations are compared with experiments to validate the proposed FE procedure.

Keywords: elasto-viscoplastic constitutive model, Bodner-Partom, FEM

1. Introduction

Although a number of constitutive equations have been developed for elasto-viscoplastic deformations of materials (see *e.g.* [1] or [2]), engineering applications of the majority of the models are limited due to difficulties in identification of a large number of material parameters. The B-P constitutive model, proposed by Bodner and Partom [3] in the 1970s, is one of the unified theories, used in many practical engineering applications. A brief review of applications of the B-P model is given below.

A simple, unconditionally stable numerical procedure for time integration of the flow rule for large plastic deformation of metals was developed by Rubin [4]. The crack tip temperature due to near-tip dissipation of mechanical energy for a crack propagating in a viscoplastic material was investigated by Sung and Achenbach [5].

The problem of the elasto-viscoplastic dynamic behaviour of geometrically nonlinear plates and shells, under the assumption of small strains and moderate rotations, was investigated by Kłosowski *et al.* [6]. The elasto-viscoplastic equations of B-P was

modified by Rubin and Bodner [7] to model strong non-proportional loading paths such as those experienced in corner turning tests and certain cases of inelastic buckling. A numerical method for the implementation of a micromechanical model capable of predicting the thermomechanical response of laminated metal matrix composites in the presence of damage development with the B-P model was developed by Lissenden and Herakovich [8]. In [9], Mahnken and Stein presented a unified strategy for identification of material parameters of the Chaboche [10], Bodner-Partom [3] and Steck [11] viscoplastic constitutive models from uniaxial tests. Several explicit integration algorithms with self-adaptive time integration strategies was developed and investigated by Arya [12] and applied to the Freed-Verrilli [13] and B-P viscoplastic models. The numerous computations performed showed that, for comparable accuracy, the efficiency of an integration algorithm depends significantly on the type of application. Zhang and Moore [14] used the B-P and the extended Kelvin models to describe the behaviour of high-density polyethylene. Foringer *et al.* [15] described fatigue life modelling of titanium-based MMCs (metal-matrix composites), on the examples of SCS-6/Timetal21s and SCS-6/Ti-15-3. Sansour and Kollmann [16] considered the theory and numerics of finite inelastic deformations. They employed evolution equations of the Bodner-Partom type with the concept of multiplicative decomposition of the deformation gradient and various numerical examples of finite strain deformations. Kroupa and Bartsch [17] investigated an improved formulation for the viscoplastic response of the Timetalt21S matrix. Their modifications to the Bodner-Partom constitutive equations improved flexibility in fitting a larger strain-rate range than previously available. The material parameters of the isotropic form of the Bodner-Partom model were found as functions of temperature for the eutectic solder by Skipor and Harren [18]. The resulting temperature-dependent viscoplastic description was implemented in an infinitesimal-strain, incrementally-linear finite element method.

Sansour and Kollmann [19] investigated large viscoplastic deformations of shells with the constitutive model based on the concept of unified Bodner-Partom evolution constitutive equations. They proposed an algorithm for the evaluation of the exponential map for non-symmetric arguments and a closed form of the tangent operator. An enhanced strain FEM and various examples of large shell deformations were also given, including loading-unloading cycles. Esat *et al.* [20] presented an implementation of the unified Bodner-Partom theory in a three-dimensional finite-element program analysing anisotropic inelastic behaviour of selected metals. A comparative study of vibrations of elasto-viscoplastic circular plates subjected to shock-wave impulses were presented by Kłosowski *et al.* [21]. Woznica and Kłosowski [22] evaluated material parameters for viscoplastic Chaboche and Bodner-Partom constitutive equations using tensile tests.

Frank and Brockman [23] developed the Bodner-Partom constitutive equations for glassy polymers. Their model was implemented into an FEA program and appropriate parameters were identified for a polycarbonate. Barta and Jaber [24] used the Litonski-Batra, Johnson-Cook, Bodner-Partom and power law thermo-viscoplastic constitutive relations to model the thermo-viscoplastic response of an HY-100 steel material. A numerical tool was developed by Aa *et al.* [25] to analyse the wall ironing process of sheet metal coated with a polymer layer. Under industrial processing conditions, both sheet metal and polymer coating exhibit elasto-viscoplastic behaviour.

The material behaviour of the polymer layers was described by the Leonov model [26] and that of the metal sheet – by the B-P model. A framework of additive models of finite strain plasticity and viscoplasticity was developed by Sansour and Wagner ([27, 28]). They modified the Bodner-Partom evolution equations so that they fit into the theoretical framework adopted and fully developed their numerical treatment of the problem.

Andersson *et al.* [29] performed crack growth tests on specimens with rectangular cross-section of Incotel 718 in order to examine the low-cycle fatigue behaviour. The material was described in terms of the Bodner-Partom viscoplastic constitutive equations and the material parameters were found by fitting simulations to experimental data. An FE implementation of Bodner's unified elastic-viscoplastic theory for the analysis of metal matrix composites was presented by Shati *et al.* [30]. An original model of circular fibres embedded in a square array of matrix material was chosen for their investigation.

Barta and Chen [31] investigated thermomechanical deformations of a steel block deformed in simple shear and modelled the thermo-viscoplastic response of the material. Song *et al.* [32] presented an application of the Bodner-Partom model to FEA of high velocity impact. The material parameters were determined on the basis of experiments with Hopkins bar tests. Bodner [33] described the unified constitutive theory for elasto-viscoelastic material behaviour at high and very high strain rates. A framework for an implicit implementation of the Bodner-Partom material model was presented by Anderson [34]. Batra *et al.* [35] numerically investigated the effect of the shape of the notch-tip and the presence of a hole ahead of a circular notch-tip on the initiation and transition speed of the failure mode. Jiang *et al.* [36] developed a B-P constitutive model for predicting the thermal and mechanical responses of a cobalt-based ULTIMET alloy subjected to cyclic deformation. The model was constructed in the light of internal state variables, developed to characterize the inelastic strain of the material during cyclic loading.

Kłosowski and Woznica [37] investigated the influence of higher order terms, which should be taken into account in the shell strain-displacement relations according to moderate or large rotations theories. They also discussed various types of viscoplastic constitutive models applied to FE problems. Hart *et al.* [38] introduced stochastic methods to describe the influence of scattering test data on the identification of material parameters for the B-P viscoplastic constitutive model. The material parameters were determined for AINSI SS 316 stainless steel at 600°C on the basis of creep tests, constant strain rate tension tests and cyclic tension-compression tests. Kłosowski *et al.* [39] presented the results of experiments on the Panama technical fabric performed to identify the inelastic properties of warp and weft. The B-P and Chaboche viscoplastic models were applied to describe their properties.

In order to predict the inelastic deformations of shock wave loaded plates' simulations, Stoffel ([40, 41]) used the viscoplastic constitutive equations of Chaboche and B-P combined with a structural theory. Zaïri *et al.* [42] applied a unified elastic-viscoplastic B-P model to non-linear modelling of glass polymers. They showed the modified B-P model associated with the original version to be sufficiently flexible to permit the modelling of the representative amorphous glassy polymer's response.

Experimental tests in tension on a RT-PMMA material were performed by Zaïri *et al.* [43] under various constant strain rates.

2. Bodner-Partom constitutive equations

The Bodner-Partom model [3] is based on the assumption of strain additivity, where strain rate $\dot{\boldsymbol{\varepsilon}}$ is decomposed into its elastic, $\dot{\boldsymbol{\varepsilon}}^E$, and inelastic, $\dot{\boldsymbol{\varepsilon}}^I$, strain elements:

$$\dot{\boldsymbol{\varepsilon}} = \dot{\boldsymbol{\varepsilon}}^E + \dot{\boldsymbol{\varepsilon}}^I. \tag{1}$$

Generally, strain rate $\dot{\boldsymbol{\sigma}}$ is specified by the time derivate of Hooke's law as:

$$\dot{\boldsymbol{\sigma}} = \mathbf{B} : \dot{\boldsymbol{\varepsilon}}^E = \mathbf{B} : \left(\dot{\boldsymbol{\varepsilon}} - \dot{\boldsymbol{\varepsilon}}^I\right), \tag{2}$$

where $\mathbf{B}$ is the tensor of elastic modules. In a practical numerical algorithm, the stress in time t may also be written in the form:

$${}^t\boldsymbol{\sigma} = {}^{t-\Delta t}\boldsymbol{\sigma} + \Delta\boldsymbol{\sigma}, \tag{3}$$

where stress increment $\Delta\boldsymbol{\sigma}$ is specified by the following equation:

$$\Delta\boldsymbol{\sigma} = \mathbf{B} : \Delta\boldsymbol{\varepsilon}^E = \mathbf{B} : \left(\Delta\boldsymbol{\varepsilon} - \Delta\boldsymbol{\varepsilon}^I\right). \tag{4}$$

The inelastic strain rate, $\dot{\boldsymbol{\varepsilon}}^I$, of the Bodner-Partom model is given by the equation:

$$\dot{\boldsymbol{\varepsilon}}^I = \frac{3}{2}\,\dot{p}\,\frac{\boldsymbol{\sigma}'}{J(\boldsymbol{\sigma}')}, \tag{5}$$

where $\dot{p}$, $\boldsymbol{\sigma}'$ and $J(\boldsymbol{\sigma}') = \sqrt{\frac{3}{2}(\boldsymbol{\sigma}' : \boldsymbol{\sigma}')}$ are the equivalent plastic strain, the deviatoric stress tensor and the stress invariant, respectively. The rate of the equivalent plastic strain, $\dot{p}$, is defined by:

$$\dot{p} = \frac{2}{\sqrt{3}}\,D_0 \cdot \exp\left[-\frac{1}{2}\left(\frac{R + \left(\mathbf{X} : \dfrac{\boldsymbol{\sigma}}{J(\boldsymbol{\sigma})}\right)}{J(\boldsymbol{\sigma}')}\right)^{2n} \cdot \frac{n+1}{n}\right], \tag{6}$$

where D_0 and n are material parameters and represent the limiting plastic strain rate and the strain rate sensitivity parameter. The equivalent strain rate, $\dot{p}$, may be found in the literature in another form as well, *viz.*:

$$\dot{p} = \frac{2}{\sqrt{3}}\,D_0 \cdot \exp\left[-\frac{1}{2}\left(\frac{R + \left(\mathbf{X} : \dfrac{\boldsymbol{\sigma}}{J(\boldsymbol{\sigma})}\right)}{J(\boldsymbol{\sigma}')}\right)^{2n}\right]. \tag{7}$$

Isotropic and kinematic hardenings are specified by the following equations:

$$\dot{R} = m_1\,(Z_1 - R)\,\dot{W}^I - A_1\,Z_1\left(\frac{R - Z_2}{Z_1}\right)^{r_1}, \tag{8}$$

$$\dot{\mathbf{X}} = m_2\left(\frac{3}{2}\,Z_3\,\frac{\boldsymbol{\sigma}}{J(\boldsymbol{\sigma})} - \mathbf{X}\right)\dot{W}^I - A_2\,Z_1\,\frac{3}{2}\left(\frac{\frac{2}{3}J(\mathbf{X})}{Z_1}\right)^{r_2}\frac{\mathbf{X}}{J(\mathbf{X})}, \tag{9}$$

where m_1, A_1, r_1 are the hardening rate coefficient, the recovery coefficient and the recovery exponent for isotropic hardening, while m_2, A_2, r_2 are the hardening rate

coefficient, the recovery coefficient and the recovery exponent for kinematic hardening, respectively. The parameters are as follows: Z_1 – the limiting (maximum) value for isotropic hardening, Z_2 – the fully recovered (minimum) value for isotropic hardening, and Z_3 – the limiting (maximum) value for kinematic hardening. The initial value of isotropic hardening is $R(t=0)=Z_0$. It should be noted that the plastic work rate, $\dot{W}^I$, is calculated from the following equation:

$$\dot{W}^I = \boldsymbol{\sigma} : \dot{\boldsymbol{\varepsilon}}^I. \tag{10}$$

3. Numerical examples

The MSC.Marc system in numerical calculations was used. However, as the standard MSC.Marc system does not support the Bodner-Partom material models, user-defined UVSCPL subroutines [44] were used to apply the Bodner-Partom model to the system, specifying the inelastic strain rate and stress increments. The fundamental part of the algorithm used in the implementation of UVSCPL subroutines is presented in Figure 1 in the form of a flow graph.

$$
\begin{aligned}
&[\text{step } 1] \rightarrow \begin{bmatrix} \Delta\mathbf{X} = \frac{\Delta t}{2}\left(\dot{\mathbf{X}}_{j-1} + \dot{\mathbf{X}}_j\right), & \mathbf{X}_j = \mathbf{X}_{j-1} + \Delta\mathbf{X} \\ \Delta R = \frac{\Delta t}{2}\left(\dot{R}_{j-1} + \dot{R}_j\right), & R_j = R_{j-1} + \Delta R \end{bmatrix} \\
&[\text{step } 2] \rightarrow \left[\boldsymbol{\sigma}'_j,\, J(\boldsymbol{\sigma}'_j),\, J(\boldsymbol{\sigma}_j),\, J(\mathbf{X}_j)\right] \\
&[\text{step } 3] \rightarrow \left[\dot{p}_j = \frac{2}{\sqrt{3}} D_0 \cdot \exp\left[-\frac{1}{2}\left(\frac{R + \left(\mathbf{X}_j : \frac{\boldsymbol{\sigma}_j}{J(\boldsymbol{\sigma}_j)}\right)}{J\left(\boldsymbol{\sigma}'_j\right)}\right)^{2n} \cdot \frac{n+1}{n}\right]\right] \\
&[\text{step } 4] \rightarrow \left[\dot{\boldsymbol{\varepsilon}}^I_j = \frac{3}{2}\dot{p}\frac{\boldsymbol{\sigma}'_j}{J\left(\boldsymbol{\sigma}'_j\right)}\right] \\
&[\text{step } 5] \rightarrow \left[\dot{W}^I_j = \boldsymbol{\sigma} : \dot{\boldsymbol{\varepsilon}}^I_j\right] \\
&[\text{step } 6] \rightarrow \left[\dot{\mathbf{X}}_j = m_2\left(\frac{3}{2} Z_3 \frac{\boldsymbol{\sigma}_j}{J(\boldsymbol{\sigma}_j)} - \mathbf{X}_j\right)\dot{W}^I_j - A_2\, Z_1\, \frac{3}{2}\left(\frac{\frac{2}{3}J(\mathbf{X}_j)}{Z_1}\right)^{r_2} \frac{\mathbf{X}_j}{J(\mathbf{X}_j)}\right] \\
&[\text{step } 7] \rightarrow \left[\dot{R}_j = m_1\left(Z_1 - R_j\right)\dot{W}^I_j - A_1\, Z_1\left(\frac{R_j + Z_2}{Z_1}\right)^{r_1}\right] \\
&[\text{step } 8] \rightarrow \left[\Delta\boldsymbol{\varepsilon}^I_j = \dot{\boldsymbol{\varepsilon}}^I_j \cdot \Delta t_j\right] \\
&[\text{step } 9] \rightarrow \left[\Delta\boldsymbol{\sigma}_j = \mathbf{B}\left(\Delta\boldsymbol{\varepsilon}_j - \Delta\boldsymbol{\varepsilon}^I_j\right)\right]
\end{aligned}
$$

Figure 1. Flow graph of the UVSCPL subroutine of the Bodner-Partom model

3.1. Test 1

Numerical calculations were performed for simple shell, solid and truss structures. A four-node thin-shell element (Element 139, [45]), a three-dimensional eight-node isoparametric solid element (Element 7, [45]) and a three-dimensional two-node straight truss element (Element 9, [45]) were applied. The geometry and boundary conditions of these structures were assumed in order to compare the obtained numerical results with the uniaxial tension tests performed at the Department of General

Table 1. Parameters for the Bodner-Partom model for steel at 20°C

	T [°C]	E [GPa]	ν [–]	D_0 [s^{-1}]	n [–]	Z_0 [MPa]	m_1 [MPa^{-1}]	Z_1 [MPa]
Steel, [46]	20	223	0.3	$1\cdot10^4$	9.61	259.38	0.068	422.90
	A_1 [s^{-1}]	Z_2 [MPa]	r_1 [–]	m_2 [MPa^{-1}]	Z_3 [MPa]	A_2 [s^{-1}]	r_2 [–]	$\dot{p}$
Steel, [46]	0.0	0.0	0.0	1.82	21.35	0.0	0.0	Eq. (6)

Mechanics of RWTH Aachen (see [46] for details). Parameters for the Bodner-Partom model were taken for steel at 20°C (see Table 1).

The graphs of stress versus strain for the strain rate of $\dot{\varepsilon} = 1\cdot10^{-2}\text{s}^{-1}$ are given in Figure 2. There is good agreement between the stress-strain relations obtained from MSC.Marc calculations and laboratory tests. It should be noted that the results are the same for various types of finite elements applied in the numerical calculations. This simple test confirms that the Bodner-Partom equations have correctly introduced to the MSC.Marc system using the UVSCPL subroutine.

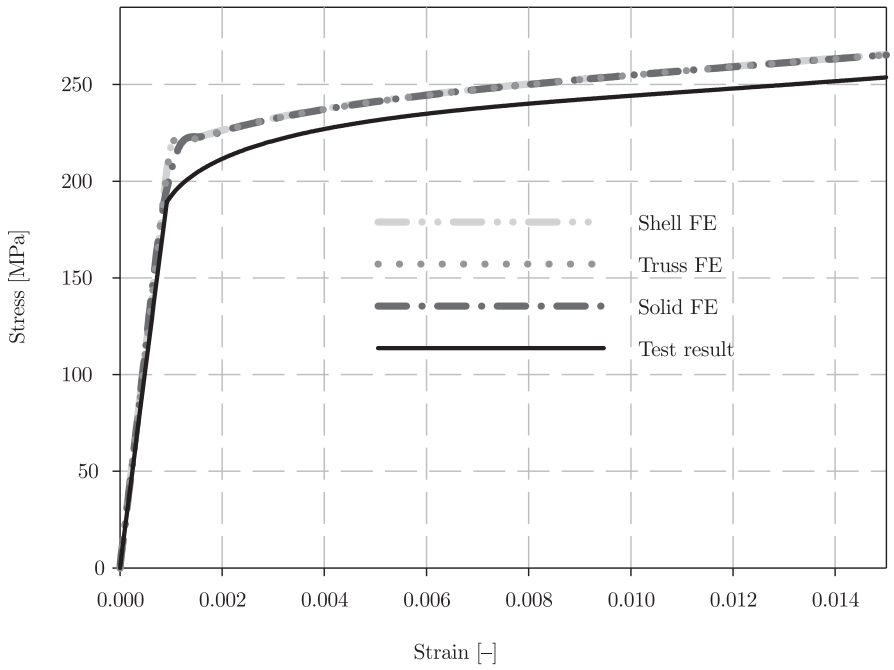

Figure 2. Results of numerical simulations of uniaxial tension tests

3.2. Test 2

In this example, numerical simulations of uniaxial tension tests for various strain rates using the Bodner-Partom models are presented. The material parameters of INCO718 at 650°C (see Table 2) were taken for the Bodner-Partom model analysis. The graphs of stress versus strain for the strain rates of $\dot{\varepsilon} = 1\cdot10^{-7}\text{s}^{-1}$, $\dot{\varepsilon} = 1\cdot10^{-2}\text{s}^{-1}$ and $\dot{\varepsilon} = 1\cdot10^{-1}\text{s}^{-1}$ are shown in Figure 3.

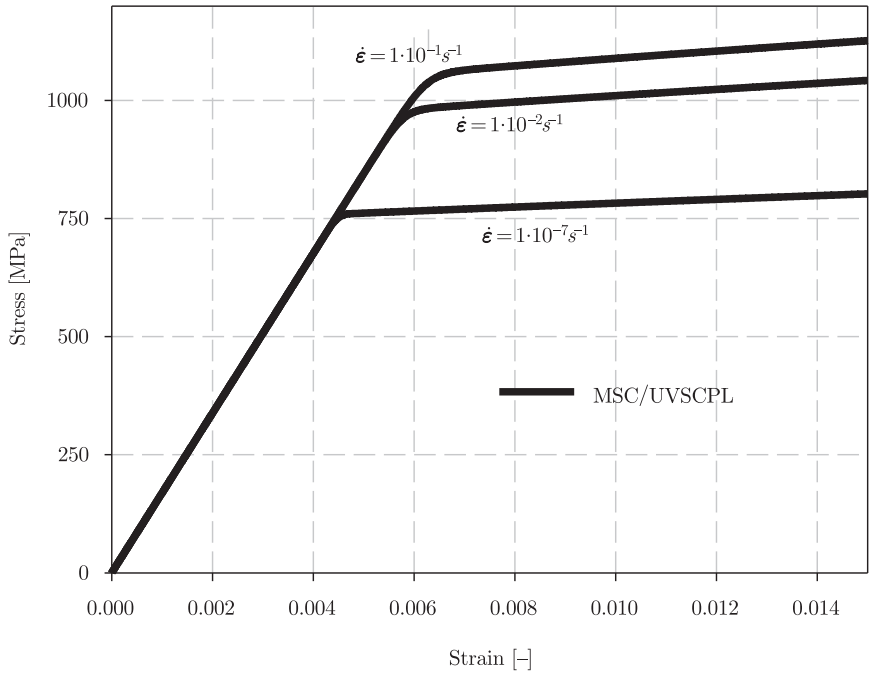

Figure 3. Numerical simulations of constant strain rate tests

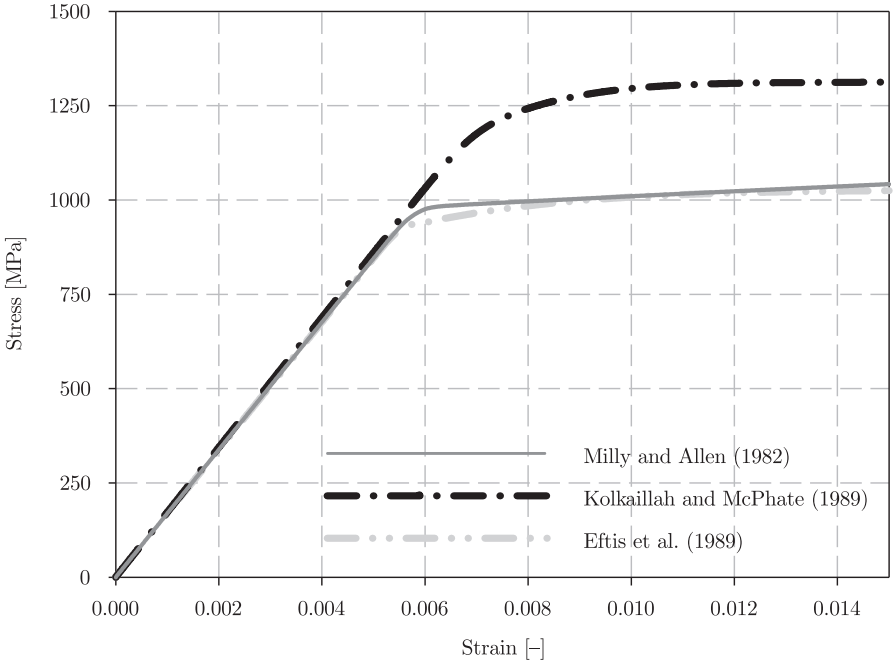

Figure 4. INCO718 results of numerical simulations for $\dot{\varepsilon} = 1 \cdot 10^{-2} \mathrm{s}^{-1}$

It should be noted that, even for the same materials under the same conditions, some material parameters vary significantly. Numerical calculations were performed with the material parameters of the chosen nickel-based INCO718 alloy at 650°C given

Table 2. Parameters for the Bodner-Partom model for nickel based the INCO718 alloy

	T [°C]	E [GPa]	ν [–]	D_0 [s^{-1}]	n [–]	Z_0 [MPa]	m_1 [MPa^{-1}]	Z_1 [MPa]
INCO718 [47]	650	172	0.3	$1.03 \cdot 10^4$	0.74	6520	0.686	7030
INCO718, [48]	650	169	0.3	10^4	1.17	3130	0.024	4140
INCO718, [49]	650	162.4	0.3	10^6	3.0	1621.5	0.42	1794.7
	A_1 [s^{-1}]	Z_2 [MPa]	r_1 [–]	m_2 [MPa^{-1}]	Z_3 [MPa]	A_2 [s^{-1}]	r_2 [–]	$\dot{p}$
INCO718, [47]	$6.82 \cdot 10^{-4}$	3690	4.73	—	—	—	$r_2 = r_1$	Eq. (6)
INCO718, [48]	$1.10 \cdot 10^{-4}$	2760	2.86	—	—	—	$r_2 = r_1$	Eq. (6)
INCO718, [49]	$1.50 \cdot 10^{-3}$	718	7.0	—	—	—	$r_2 = r_1$	Eq. (6)

by Kolkaillah and McPhate [47], Eftis *et al.* [49] and Milly and Allen [48] (see Table 2 for details). The numerical simulations (see Figure 4) were performed for a constant strain rate of $\dot{\varepsilon} = 1 \cdot 10^{-2} s^{-1}$. Significant differences can be observed between the presented material constants for Bodner-Partom constitutive model analysis. Milly and Allen [48] observed hardening while Eftis *et al.* [49] noticed softening of the alloy. Kolkaillah and McPhate [47] obtained a 15% increase of yield stress for the same material in comparison with each other (see Figure 4). It is therefore necessary for detailed research to perform experimental tests and determine the material parameters for particular cases.

3.3. Test 3

In this example, the static and dynamic results of numerical analysis of a circular steel plate are investigated. Numerical analyses are compared with the experimental tests performed at the Department of General Mechanics of RWTH Aachen (see [46] for details). Due to the symmetry of geometry and loadings, only a quarter of the plate has been investigated, with proper symmetry boundary conditions at the $x = 0$ and $y = 0$ coordinates (see Figure 5). The four-node thin-shell Element 139 of [45] was used in numerical analysis.

In the calculation's first step, a static elastic analysis was performed to verify the assumed boundary conditions and the type of analysis. An elastic modulus of $E = 223\,000\,\text{MPa}$, a Poisson's ratio of $\nu = 0.3$ and plate thicknesses of $t = 0.001\,\text{m}$ were assumed. The mass density of the steel plate was taken to be $\rho = 7\,800\,\text{kg/m}^3$. Two analytical options were tested in the MSC.Marc calculations: 'LargeDisp' and 'LargeDisp + UPDATE'. The 'LargeDisp' parameter was used when MSC.Marc was applied to calculate the total Lagrangian method. The 'LargeDisp + UPDATE' was employed when MSC.Marc was applied to calculate the Cauchy stresses and true strains.

Table 3. Deflection of the plate's middle point

Pressure p [bar]	Tests [mm]	MSC.Marc		FEA [46]
		LargeDisp [mm]	LargeDisp + UPDATE [mm]	
0.5	0.490	0.493	0.508	0.427
1.0	0.830	0.792	0.826	0.714

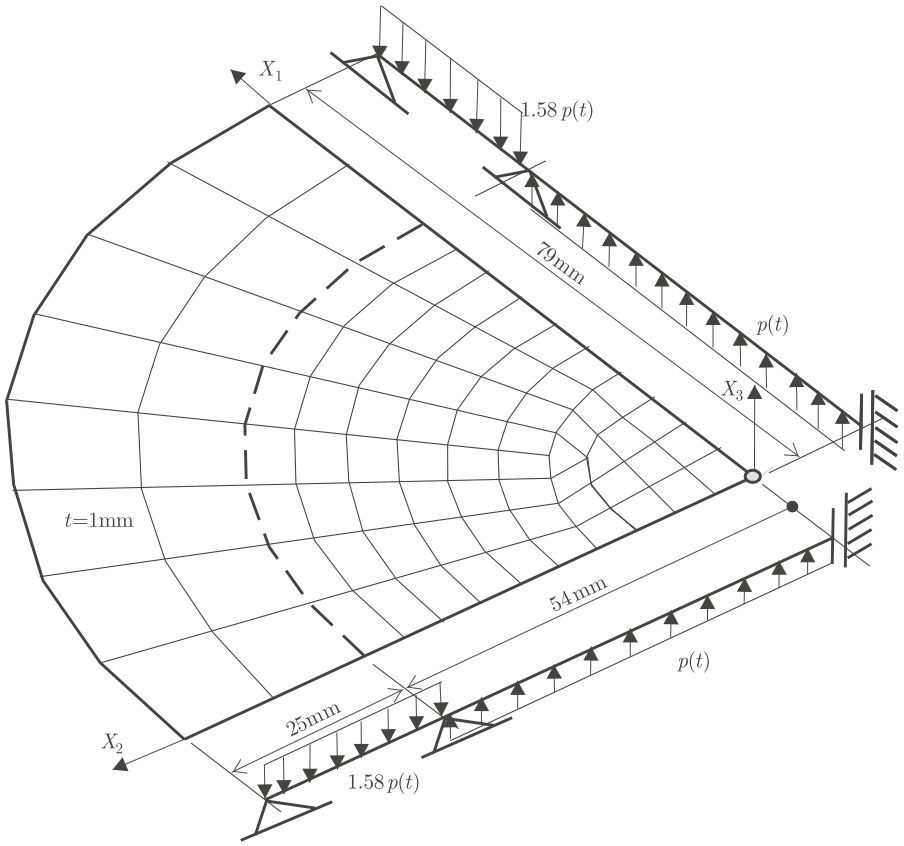

Figure 5. Visualization of the circular plate

The results of static, elastic numerical analysis are given in Table 3. The obtained results are compared with experimental measurements and FE calculations performed by Kłosowski [46], with very good agreement of vertical displacements obtained from FE calculations and experiments. The calculations confirm that the boundary conditions, values of loadings and density of mesh were assumed correctly. For the following calculations, the 'LargeDisp' option had to be used. It is worth pointing out that Kłosowski [46] used nine-node isoparametric shell elements, while four-node shell elements were applied in the present analysis.

In the second step of the numerical calculations, elastic dynamic analysis was carried out. In this case, the value of pressure was time-dependent. The experimental value of pressure, $p(t)$, for the elastic dynamic analysis was estimated through straight-line approximation and is given in Table 4. The non-linear equations of motion were integrated with the Newmark algorithm [50] with a time step of $\Delta t = 2.5 \cdot 10^{-5}$s. It was assumed in the numerical analysis that the mass matrix was lumped and damped by linear combinations of stiffness and mass matrices (Rayleigh or proportional damping):

$$\mathbf{C} = \alpha \cdot (\mathbf{K}_1 + \mathbf{K}_2) + \beta \cdot \mathbf{M}, \tag{11}$$

where α is the stiffness matrix multiplier and β is the mass matrix multiplier.

The total time of the experiment and numerical calculations was 28ms (see Figure 6). The mean value of deflection of the plate's middle point obtained from dynamic elastic numerical calculations did not exceed 10% in comparison with the experimental results. Rayleigh damping multipliers $\alpha = 5.39 \cdot 10^{-6}$ and $\beta = 15.16$ were assumed to analyze the elastic vibrations of the plate. The multipliers were established on the basis of the assumed value of critical damping, $\xi_1 = \xi_2 = 0.01$, and two known frequencies (see Table 5), in accordance with the following expressions (see *e.g.* Clough and Penzien [51]):

$$\alpha = 2 \cdot \frac{(\xi_2 \cdot \omega_2 - \xi_1 \cdot \omega_1)}{\omega_2^2 - \omega_1^2},$$
$$\beta = 2 \cdot \omega_1 \cdot \omega_2 \cdot \frac{(\xi_1 \cdot \omega_2 - \xi_2 \cdot \omega_1)}{\omega_2^2 - \omega_1^2}. \tag{12}$$

It should be noted that, when $\alpha = 0$, the highest frequencies of the constructional system are weakly damped, while they are strongly damped when $\beta = 0$.

Table 4. Time-dependent value of the calculated pressure – the elastic solution

t [ms]	0.00	3.20	3.25	4.00	4.35	6.00	18.00	28.00
p [bar]	0.00	0.00	0.70	0.70	0.85	0.90	0.90	1.00

Table 5. Comparison of frequencies of free vibrations – the elastic solution

Configuration	Initial, for $t = 0.0$ms, $p = 0.0$bar		Current, for $t = 28$ms, $p = 1.0$bar	
	[s^{-1}]	[–]	[s^{-1}]	[–]
1	704	1.0	1062	1.51
2	2477	1.0	2651	1.07

The next step of the numerical calculations was dynamic, geometrically non-linear analysis of the steel plate. The Bodner-Partom model was taken to describe the steel material, with the parameters given in Table 1. The Newmark algorithm [50] with a time step of $\Delta t = 7 \cdot 10^{-7}$s was used to integrate the non-linear equations of motion. The experimental value of pressure, $p(t)$, was estimated through straight-line approximation, like in the case of elastic dynamic analysis, and is given in Table 6.

Table 6. Time-dependent value of the calculated pressure – the inelastic solution

t [ms]	0.00	3.20	3.25	4.10	4.50	6.00	11.30	14.2	16.0	24.0	28.0
p [bar]	0.00	0.00	3.40	3.40	4.00	4.50	4.60	5.60	5.80	6.05	6.10

The results of dynamic vibrations of the steel plate's middle point are given in Figure 7 (without damping) and Figure 8 (with damping). The same values of the Rayleigh damping multipliers were assumed to analyze elastic vibrations of the plate as those assumed for elastic dynamic analysis.

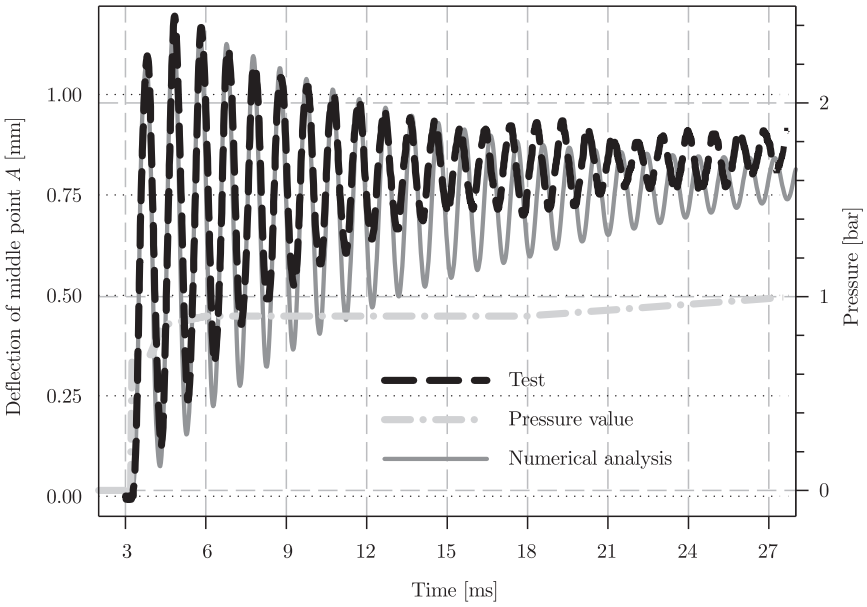

Figure 6. Elastic vibrations of the middle point

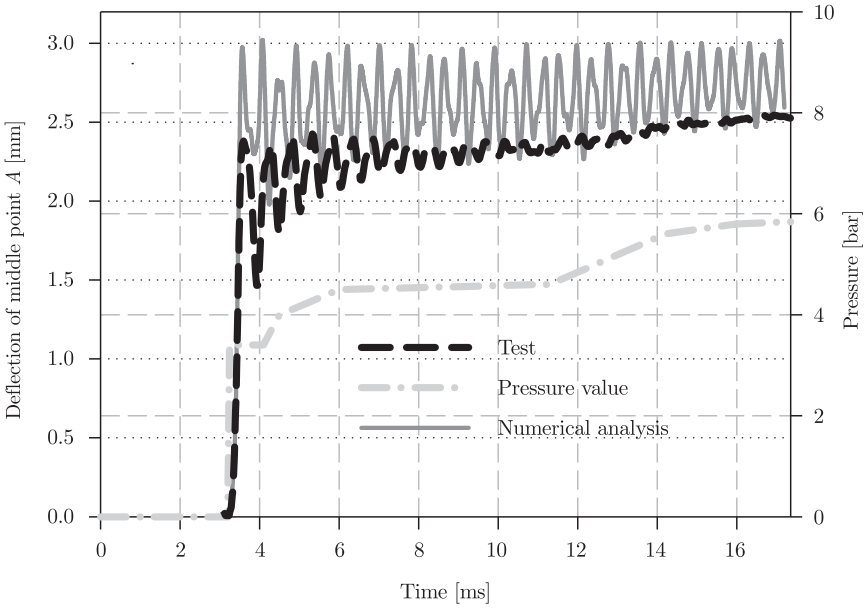

Figure 7. Inelastic vibrations of the plate's middle point (without damping)

A significant difference from the experimental results can be observed in the plate's behaviour for the case of undamped vibrations (Figure 7). When the damping factor is included, the results are very close to the functions obtained from laboratory tests (Figure 8). The simple damping model applied in the analysis and validity of material parameters (which lead to small divergences from the experiment already in the simulations of uniaxial tensile tests, see Figure 2) can explain the small differences. In the case of dynamic analysis the differences are even more emphasized.

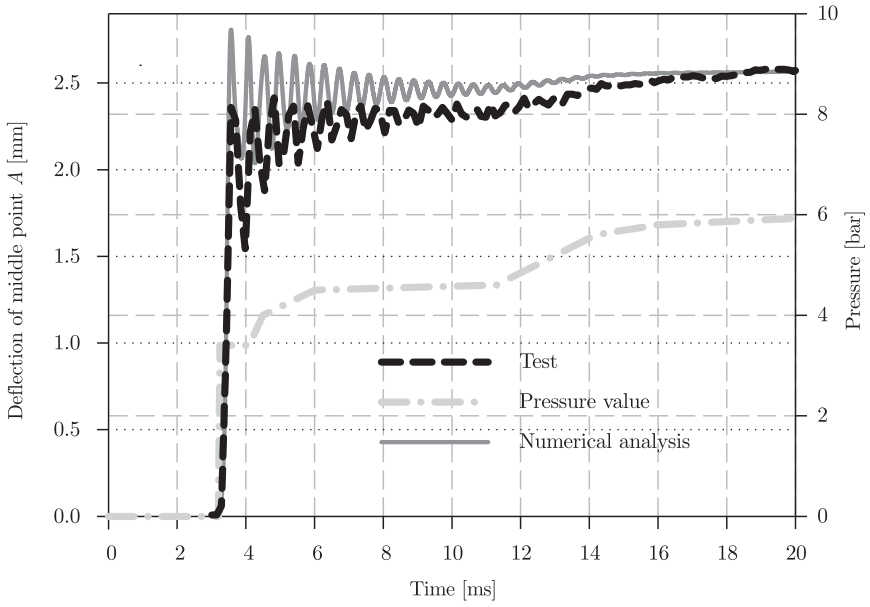

Figure 8. Inelastic vibrations of the plat'se middle point (with damping)

4. Summary

The finite element procedure for the elasto-viscoplastic non-linear static and dynamic calculations has been developed in the paper. The Bodner-Partom model can be directly applied in the calculations. The validity of the proposed FE procedure and the concept of the calculated Rayleigh damping multipliers have been confirmed. The described FE procedure with the Bodner-Partom model is open and flexible and may be implemented in many industrial applications.

Acknowledgements

The research was performed as part of Polonium 2005, a Polish-French cooperation program administrated by KBN and ÉGIDE (KBN 5598.II/2004/2005).

Calculations presented in the paper were made at the Academic Computer Centre in Gdansk (TASK).

The study was supported by the European Community under the FP5 Programme, key-action "City of Tomorrow and Cultural Heritage" (Contract No. EVK4-CT-2002-80005). This support is acknowledged with gratitude.

References

[1] Woznica K 2003 *Summer School "Simulation for Society"* (Kłosowski P, Ed.), Gdansk, Poland, pp. 77–120
[2] Woznica K 1998 *Dynamique des Structures Elasto-viscoplastique*, Cahiers de Mechanique, Lille
[3] Bodner S R and Partom Y 1975 *J. Appl. Mech.* ASME **42** 385
[4] Rubin M B 1989 *Zeitschrift für Angewandte Mathematik und Physic (ZAMP)* **40** (6) 846
[5] Sung J C and Achenbach J D 1990 *Int. J. Fracture* **44** (4) 301
[6] Kłosowski P, Weichert D and Woznica K 1995 *Arch. Appl. Mech.* **65** (5) 326
[7] Rubin M B and Bodner S R 1995 *Int. J. Solid and Structures* **32** (20) 2967
[8] Lissenden C J and Herakovich C T 1995 *Comp. Meth. Appl. Mech. and Eng.* **126** 289

[9] Mahnken R and Stein E 1996 *Int. J. Plasticity* **12** (4) 451
[10] Chaboche J L 1989 *Int. J. Plasticity* **5** 247
[11] Steck E A 1985 *Int. J. Plasticity* **1** 243
[12] Arya V K 1996 *Int. J. Num. Meth. Eng.* **39** (2) 261
[13] Freed A D and Virrilli M J 1988 *Proc. of the MECAMAT*, Besancon, Vol. I, pp. 27–39
[14] Zhang Ch and Moore I D 1997 *Polymer Engineering & Science* **37** (2) 414
[15] Foringer M A, Robertson D D and Mall S 1997 *Composites* Part B **28B** 507
[16] Sansour C and Kollmann F G 1997 *Comp. Meth. Appl. Mech. and Eng.* **146** 351
[17] Kroupa J L and Bartsch M 1998 *Composites* Part B **29B** 633
[18] Skipor A F and Harren S V 1998 *Mechanics of Time-Dependent Materials* **2** 59
[19] Sansour C and Kollmann F G 1998 *Comp. Mech.* **21** (6) 512
[20] Esat I I, Bahai H and Shati F K 1999 *Finite Elements in Analysis and Design* **32** 279
[21] Kłosowski P, Woznica K and Weichert D 2000 *European J. Mech. A/Solids* **19** 343
[22] Woznica K and Kłosowski P 2000 *Arch. Appl. Mech.* **70** (8–9) 561
[23] Frank G J and Brockman R A 2001 *Int. J. Solid and Structures* **38** 5149
[24] Barta R C and Jaber N A 2001 *Int. J. Fracture* **110** (1) 47
[25] van der Aa M A H, Schreurs P J G and Baaijens F P T 2001 *Mechanics of Materials* **33** 555
[26] Leonov A 1976 *Rheol. Acta* **15** 85
[27] Sansour C and Wagner W 2003 *Composite Structures* **81** 1583
[28] Sansour C and Wagner W 2001 *Comp. Meth. Appl. Mech. and Eng.* **191** 423
[29] Andersson H, Persson C and Hansson T 2001 *Int. J. Fatigue* **23** 817
[30] Shati F K, Esat I I and Bahai H 2001 *Finite Elements in Analysis and Design* **37** 263
[31] Barta R C and Chen L 2001 *Int. J. Plasticity* **17** 1465
[32] Song S-Ch, Duan Z-P and Tan D-W 2001 *Int. J. Solid and Structures* **38** 5215
[33] Bodner S R 2002 *Unified Plasticity for Engineering Applications*, Kluwer Academic/Plenum Publishers, New York
[34] Anderson H 2003 *Computer and Structures* **81** 1405
[35] Barta R C, Jaber N A and Malsbury M E 2003 *Int. J. Plasticity* **19** 139
[36] Jiang L, Wang H, Liaw P K, Brooks C R and Klarstrom D L 2004 *Mechanics of Materials* **36** 73
[37] Kłosowski P and Woznica K 2004 *Comp. Mech.* **34** 194
[38] Hart T, Schwan S, Lehn J and Kollmann F G 2004 *Int. J. Plasticity* **20** 1403
[39] Kłosowski P, Zagubień A and Woznica K 2004 *Arch. Appl. Mech.* **73** (9–10) 661
[40] Stoffel M 2005 *Mech. Res. Comm.* **32** 332
[41] Stoffel M 2000 *Nichtlineare Dynamic von Platten*, der Rheinisch-Westfälischen Technischen Hochschule Aachen, Aachen
[42] Zaïri F, Woznica K and Naït-Abdelaziz M 2005 *Compites Rendus Mecanique* **333** 359
[43] Zaïri F, Naït-Abdelaziz M, Woznica K and Gloaguen J-M 2005 *European J. Mech. A/Solids* **24** 169
[44] Users handbook: *MSC.Marc Volume D: User Subroutines and Special Routines*, Version 2003, MSC.Software Corporation, 2003
[45] Users handbook: *MSC.Marc Volume B: Element Library*, Version 2003, MSC.Software Corporation, 2003
[46] Kłosowski P 1999 *Non-linear Numerical Analysis and Experiments on Vibrations of Elasto-Viscoplastic Plates and Shells*, DSc Thesis, Gdansk University of Technology, Gdansk (in Polish)
[47] Kolkaillah F A and McPhate A J 1989 *J. Eng. Mech.* ASCE **10** 195
[48] Milly T M and Allen D H 1982 *A Comparative Study of Non-linear Rate-dependent Mechanical Constitutive Theories for Crystalline Solids at Elevated Temperatures*, Technical Report API-E-5-82, Virginia Polytechnic Inst. and State University, Blacksburg
[49] Eftis J, Abdel Kader M S and Jones D I 1989 *Int. J. Plasticity* **6** 1
[50] Newmark N M 1959 *J. Eng. Mechanics Division* **85** 67
[51] Clough R W and Penzien J 1993 *Dynamics of Structures*, McGraw-Hill, Inc., International Edition